Figures of Chapter 7: Ion Beam Processes

Nuclear and Electronic Stopping Cross Section

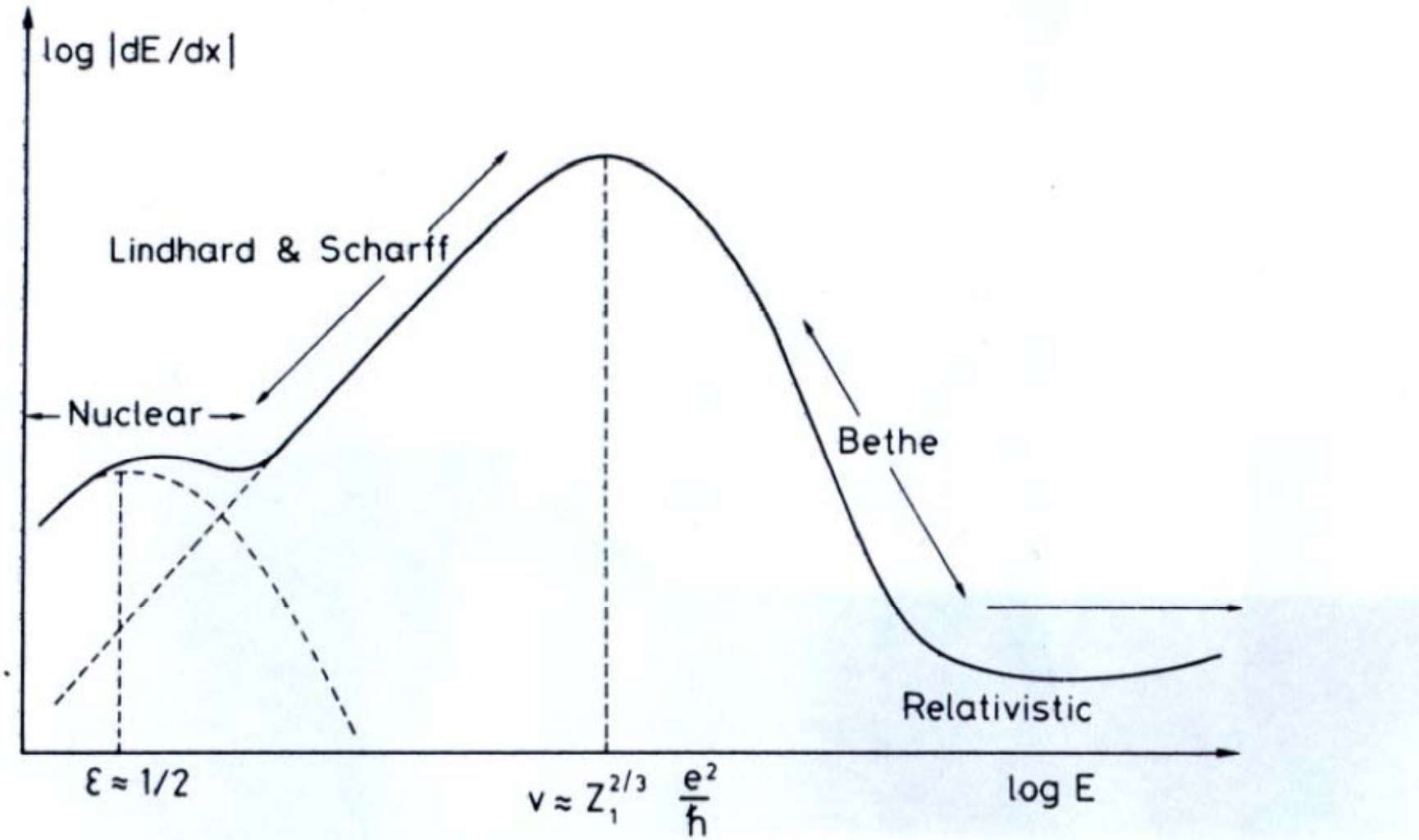

Fig. 2.7. Stopping power of an ion as a function of energy (schematically).

Fig. 7.1

Nuclear and Electronic Stopping Cross Section

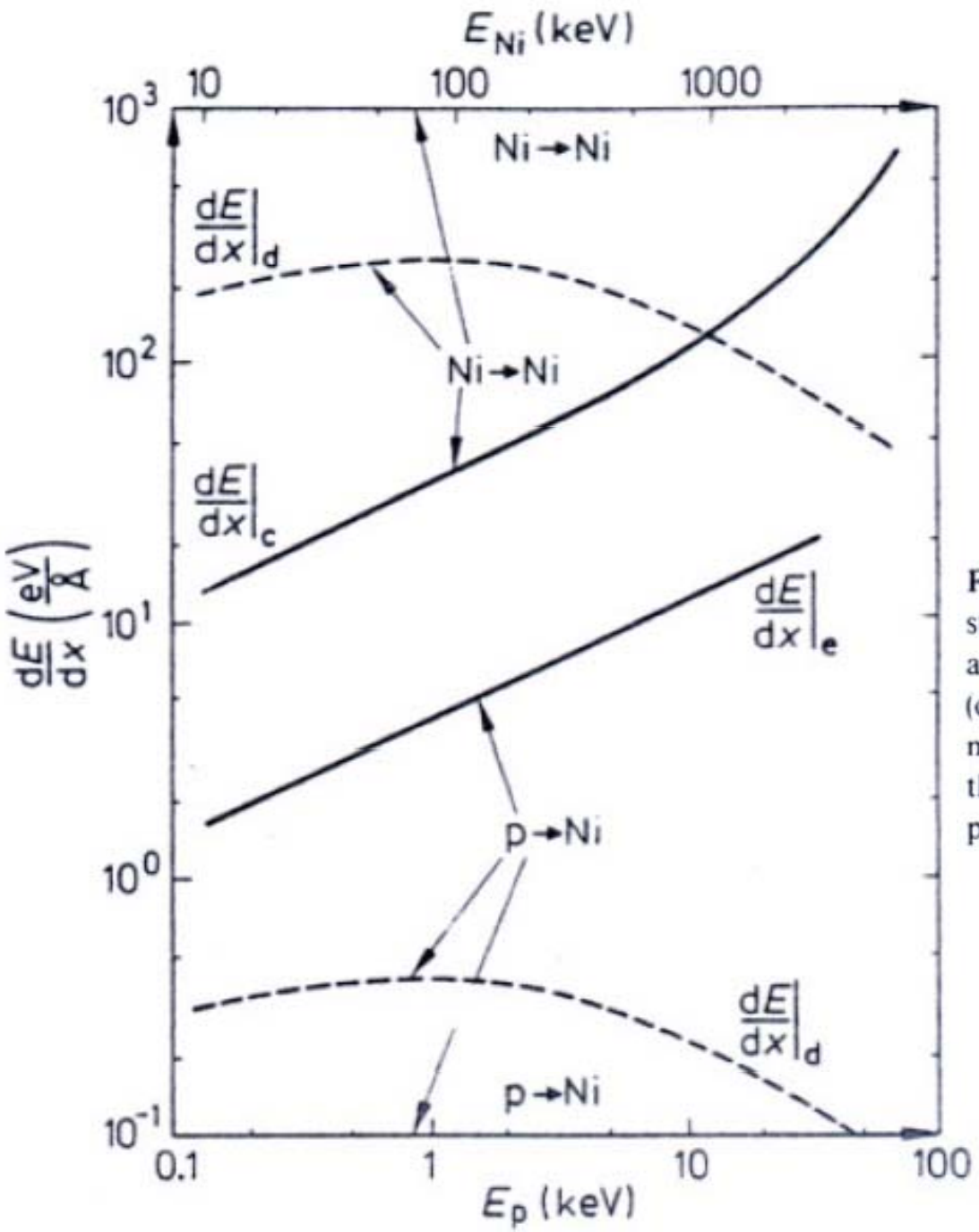

Figure 9-1. Electronic stopping $dE/dx|_e$ and nuclear stopping $dE/dx|_d$ as a function of particle energies E_p and E_{Ni} for protons and nickel ions, respectively, in Ni (calculated by the TRIM-code; Biersack and Haggmark, 1980). The energy scales are adjusted such that the reduced Lindhard energy ε is the same for both particles.

Fig. 7.2

Ion Range

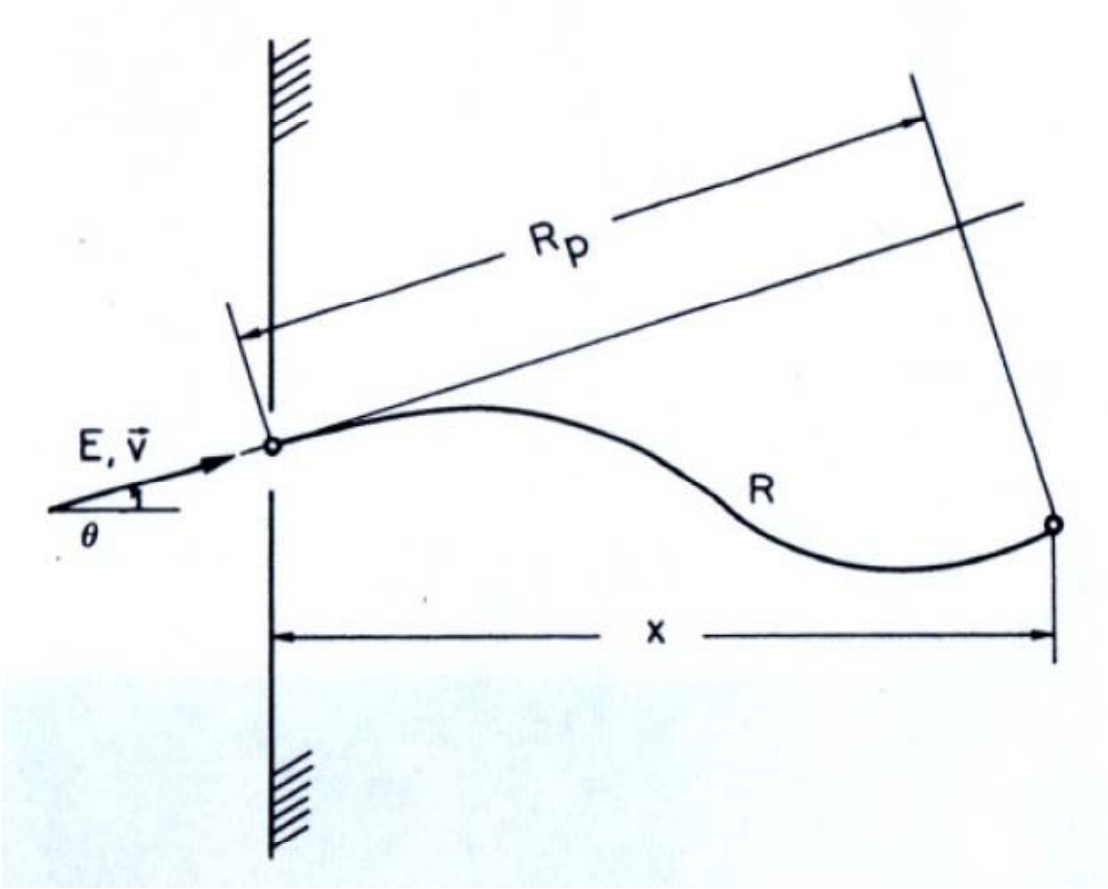

Fig. 7.3

Collision Cascade

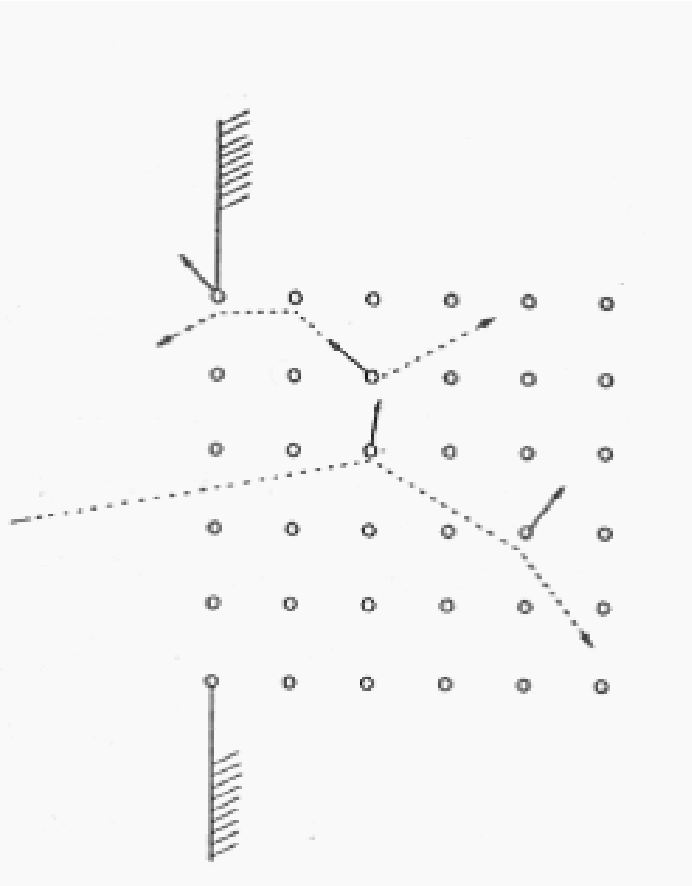

Fig. 7.4

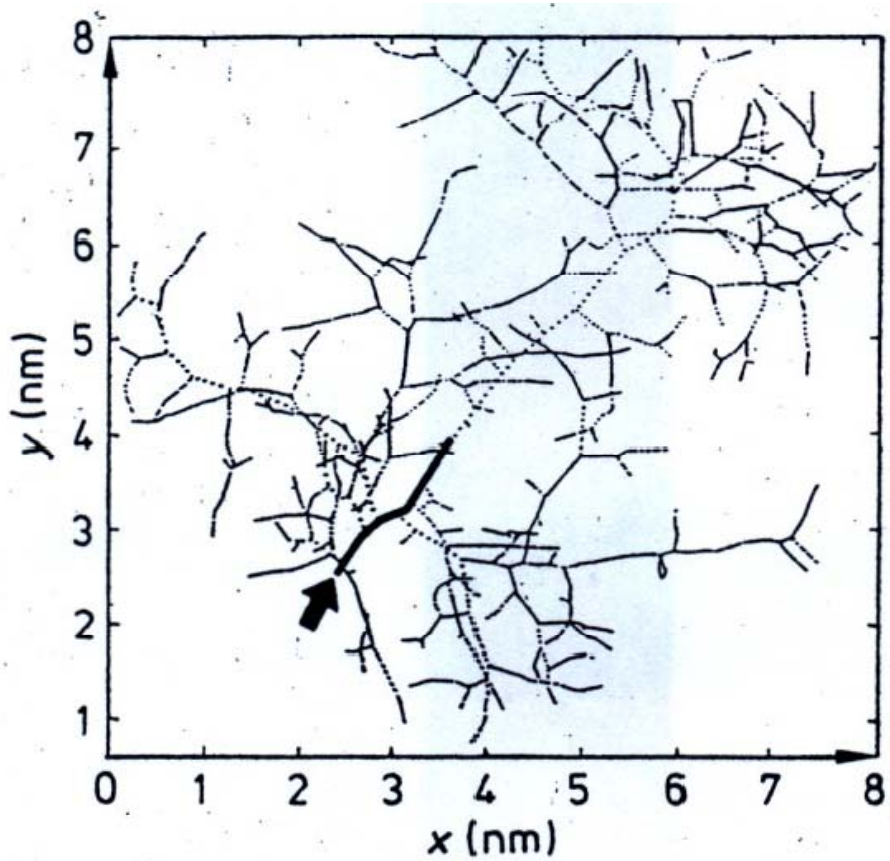

Figure 9-14. Projection on the {100} plane of the knock-on-atom trajectories calculated for a PKA with $T = 5$ keV in b.c.c. iron (Beeler, 1983). The thick line represents the trajectory of the PKA, the dotted lines those of the secondary knock-ons. Higher order knock-ons are presented by the thinner alternately solid and dashed lines.

Thermal Spike: Shock Wave and Melt for a 5keV Event in Cu Bulk

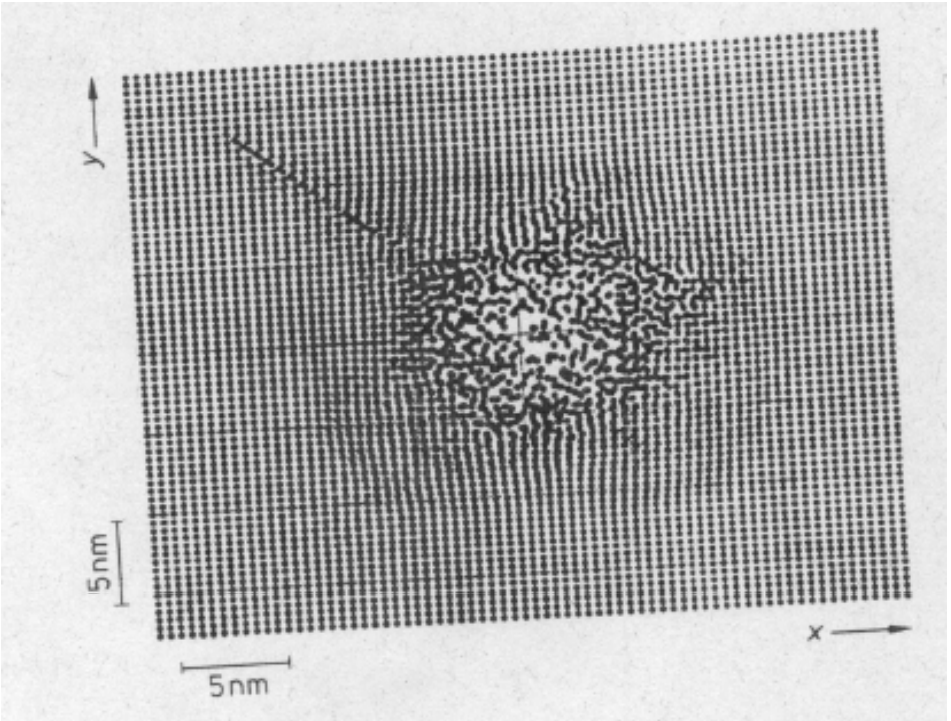

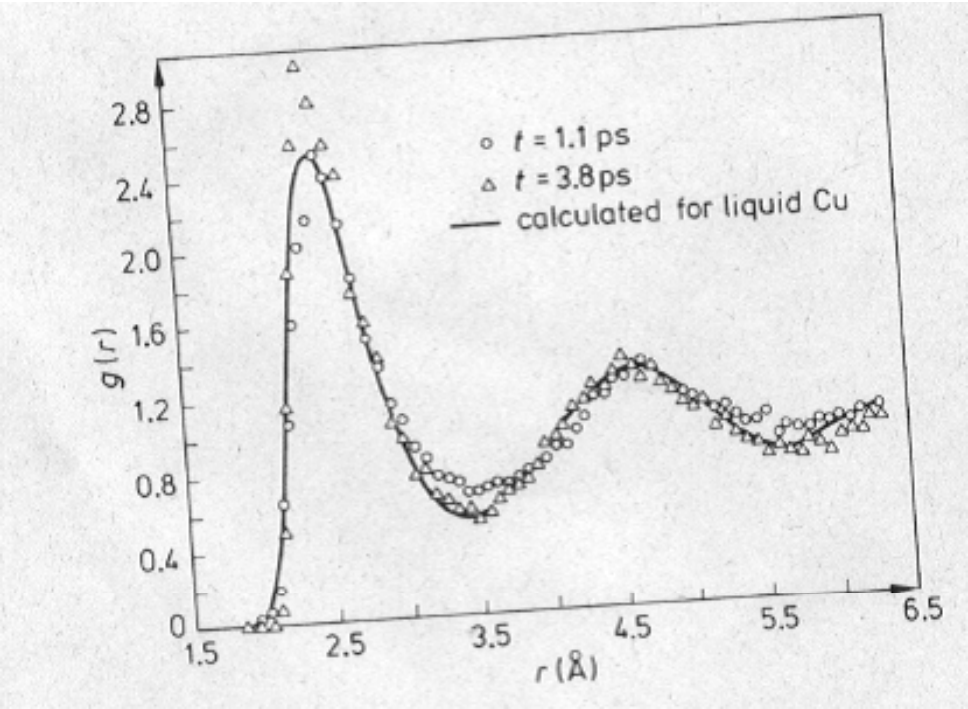

Fig. 7.5

Movie of a Thermal Spike: 16 keV Ar^+ on Au(111)

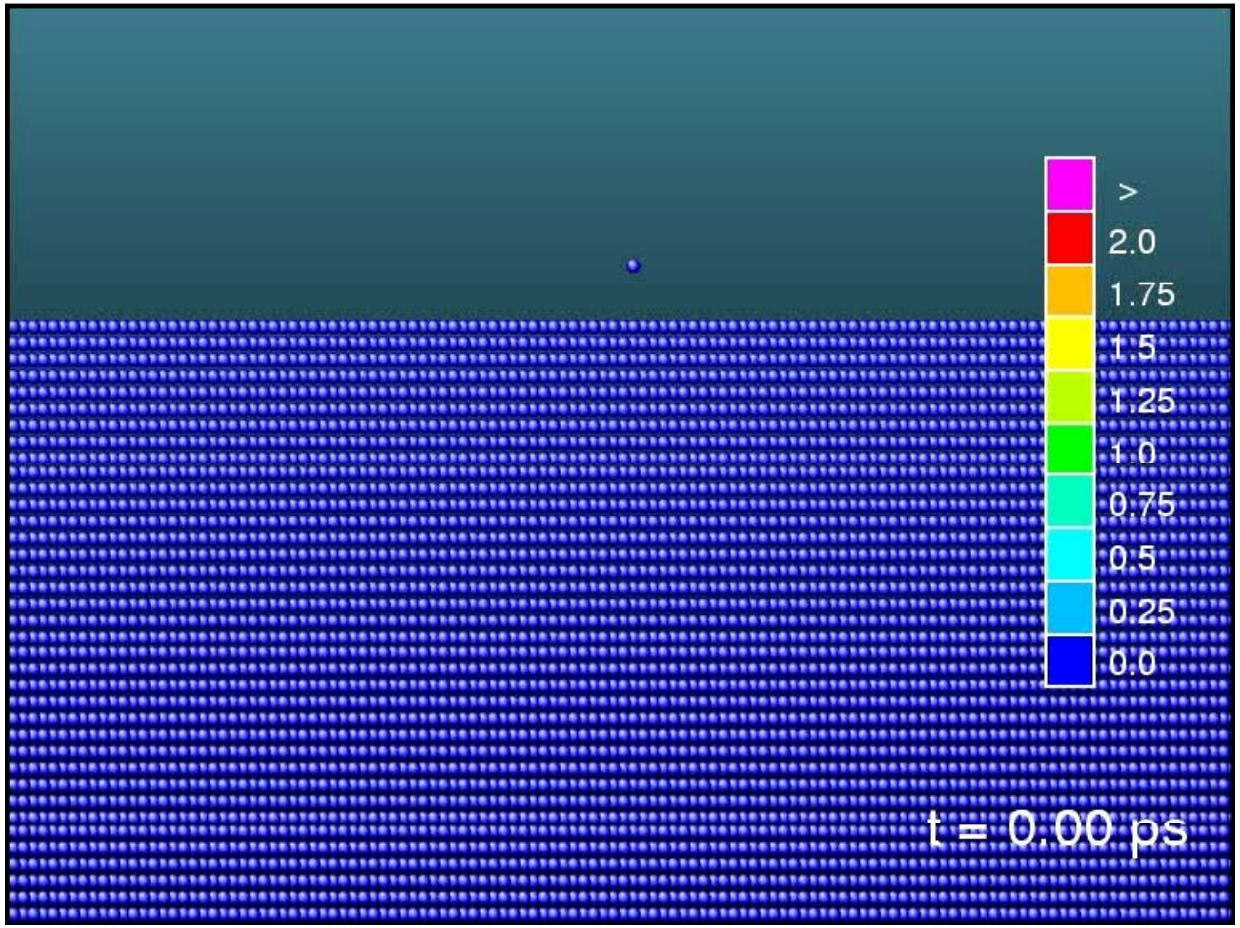

Fig. 7.6

Movie of a Thermal Spike: 16 keV Ar^+ on Au(111)

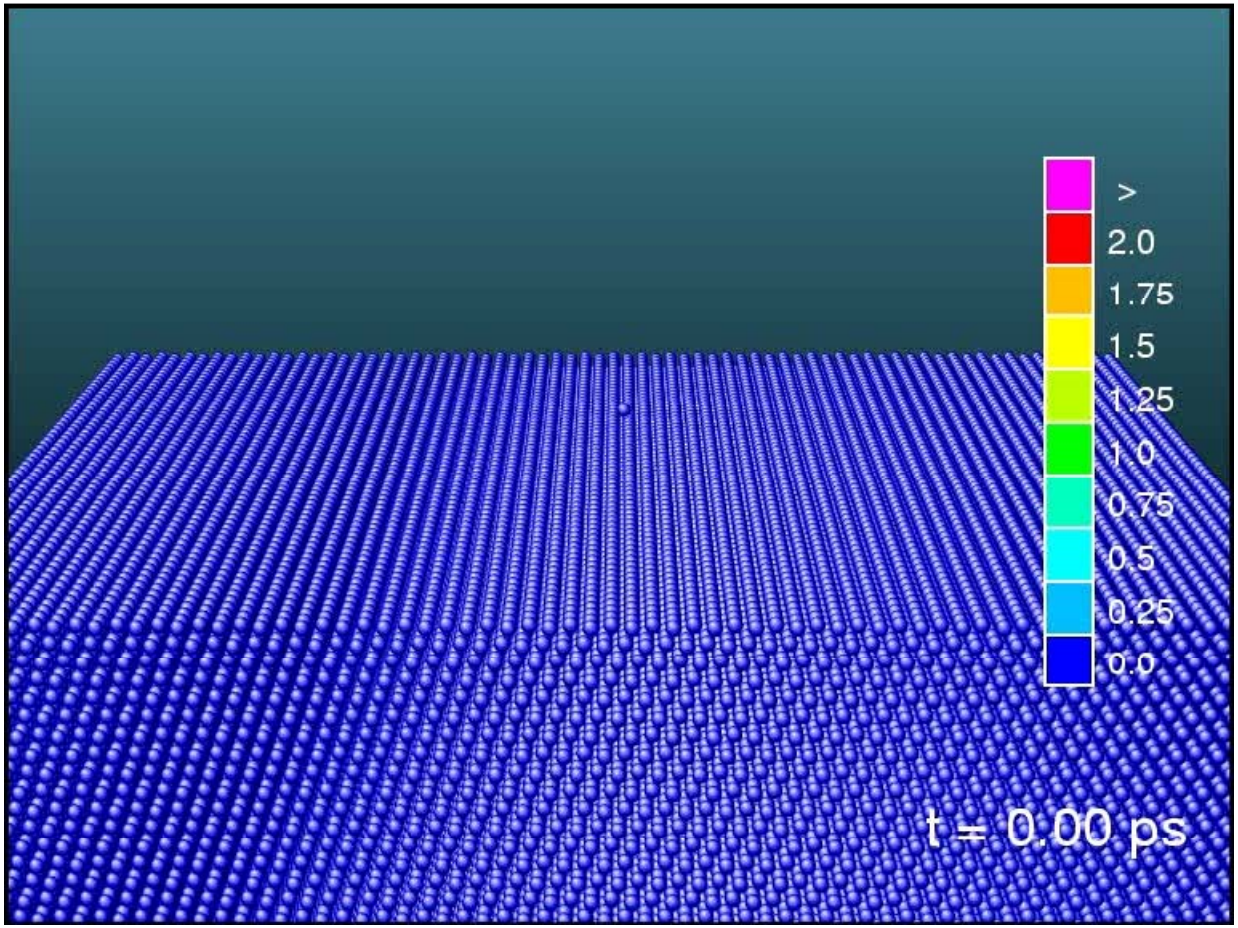

Fig. 7.7

Adatom Clusters by Thermal Spikes

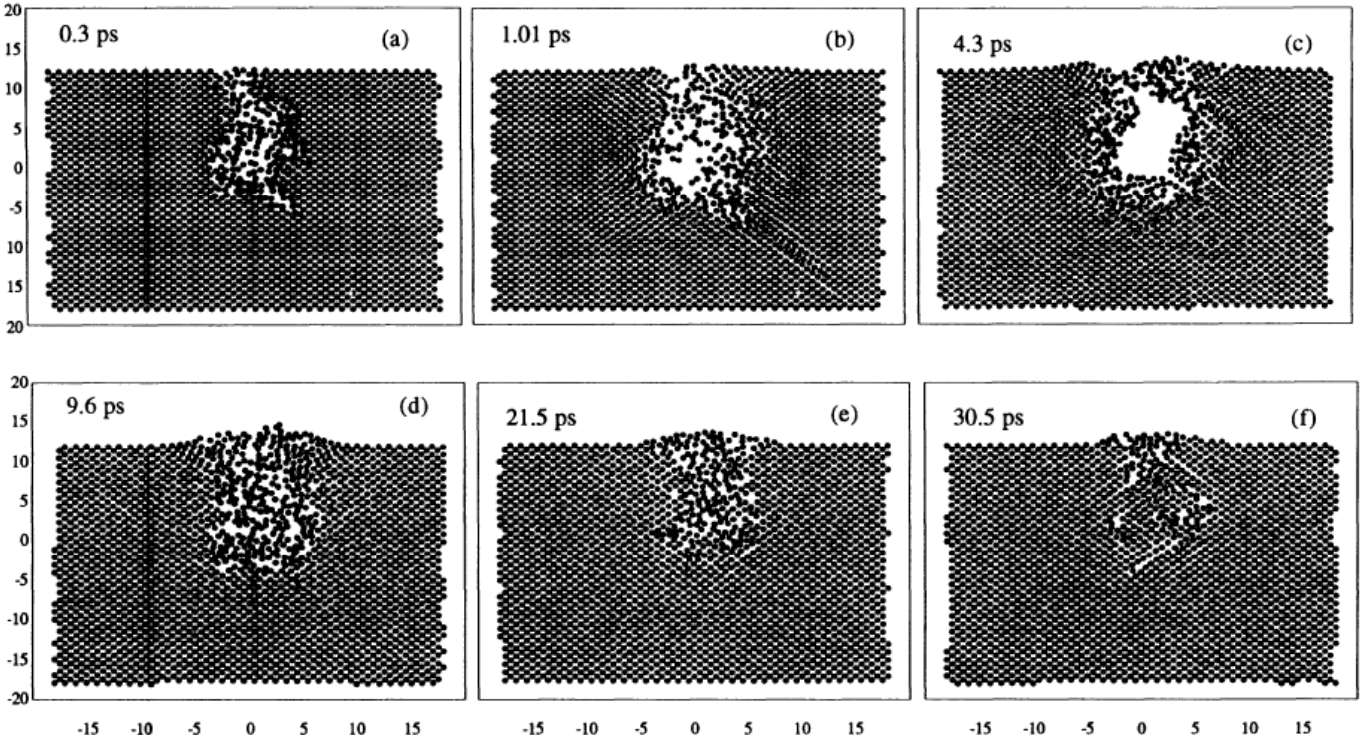

10 keV Au, 0 K

↓

Au(001)

550 adatoms

M. Ghaly and
R.S. Averback
PRL 72 (1994) 364

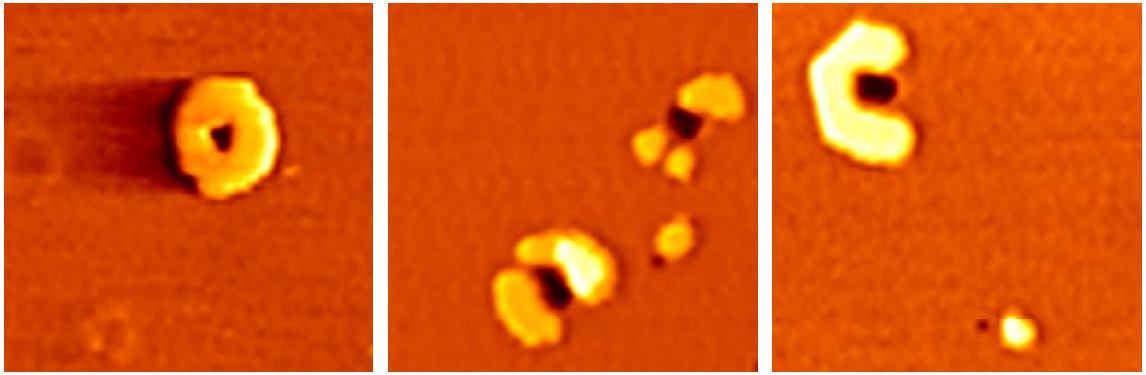

10 keV Xe^+, 300 K

Pt(111)

400 – 600 adatoms

← 210 Å →

Fig. 7.8

C. Teichert, M. Hohage, T. Michely, G. Comsa, PRL 72 (1994) 1682

Stages of Ion- Sold Interaction

Duration (ps)	Event	Result	Characteristic parameters
10^{-6}	transfer of recoil energy from irradiation particle	primary knock-on atom	T : PKA-energy T_{dam} : damage energy $d\sigma(E,T)$: cross section
10^{-6} to 0.2	slowing down of PKA, generation of a collision cascade (CC)	vacancies and low energetic recoils, subcascades	T_d : displacement threshold $N_d(I)$: number of displaced atoms n_{sc} : average number of subcascades
0.2 to 0.3	spike formation	low density, hot molten droplet, shock front	T_{sp} : max. spike temperature $V_{sp,m}$: max. melt volume $\Delta\varrho_{sp}$: atomic density deficit in spike core
0.3 to 3	spike relaxation, interstitial ejection, transition from heated to undercooled liquid core	stable interstitials (SIAs) atomic mixing	$\tau_{sp,m}$: melt lifetime in spike m : atomic mixing efficiency
3 to 10	spike core solidification and cooling to ambient temperature	depleted zone (DZ) disordered zone amorphous zone vacancy collapse	$\nu(T)$: number of stable FDs at 0 K $\xi^0(T)$: damage efficiency at 0 K η_{diso} : disordering efficiency η_{amo} : amorphization efficiency

W. Schilling, H. Ullmaier, in ;Materials Science and Technology Vol. 10, ed. R.W. Cahn, P. Haasen, K. Kramer (Verlag Chemie, Weilheim 1993)

Fig. 7.9

Evolution of an implanted string during anneling

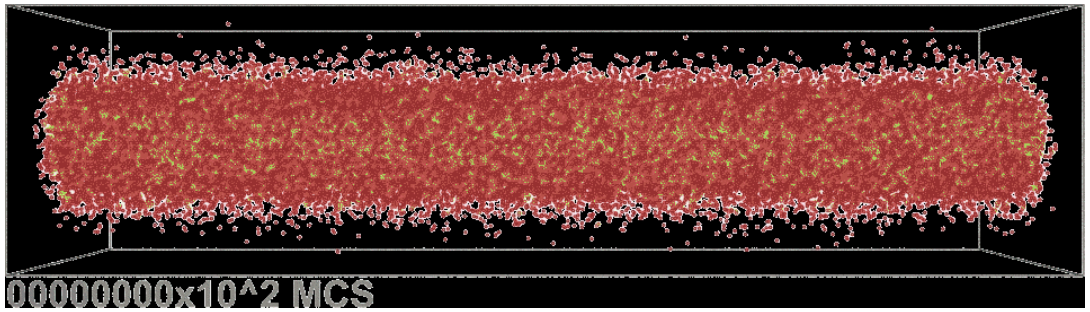

http://www.roentzsch.org/NW-IBS/index.html

Fig. 7.10

Silicon Clusters in Oxide as an Alternative Floating Gate for Flash Memories

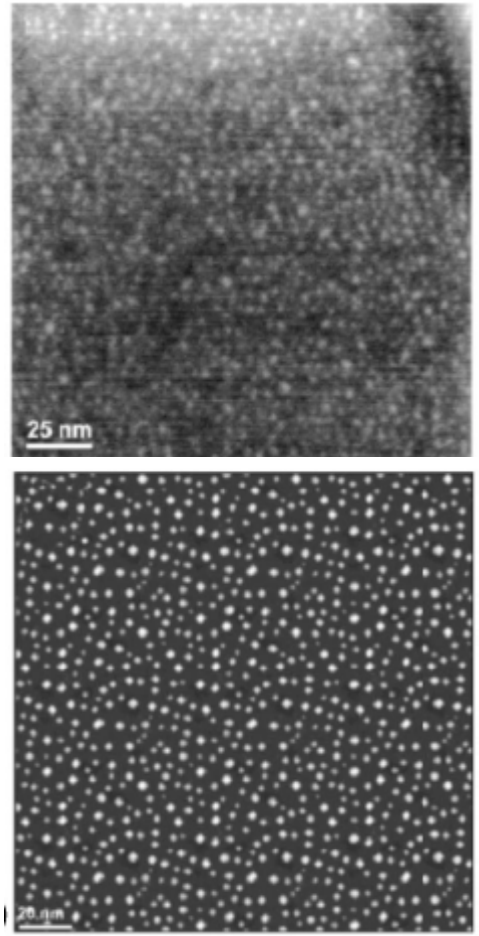

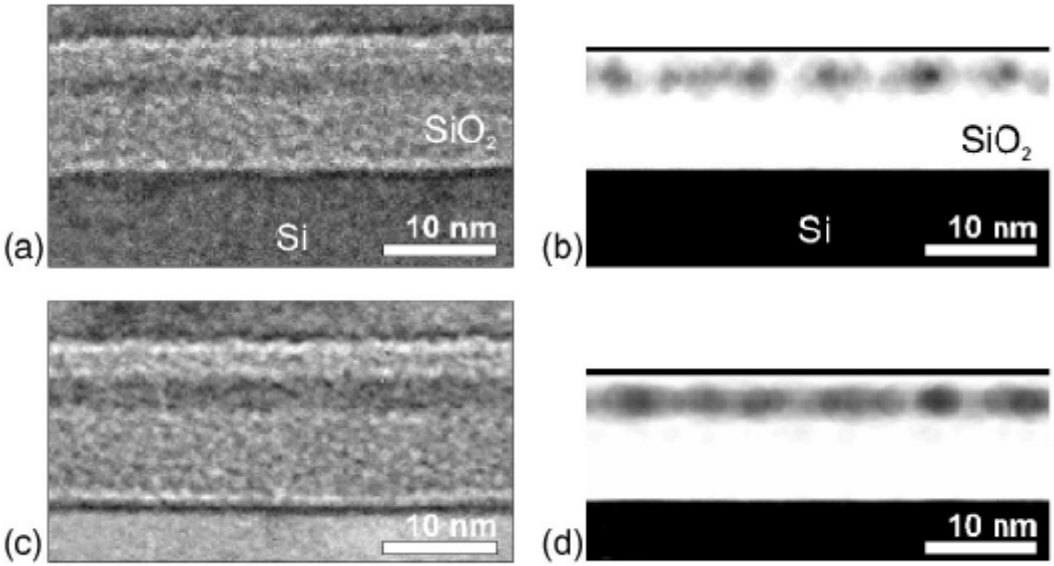

FIG. 2. Cross-section view of the layer of phase separated Si in SiO_2. Fresnel XTEM images for (a) $1 \times 10^{16} Si^+ cm^{-2}$ and (c) $2 \times 10^{16} Si^+ cm^{-2}$ are compared to cross-sectional KMC simulation snapshots for (b) $3 \times 10^{15} Si^+ cm^{-2}$ and (d) $8 \times 10^{15} Si^+ cm^{-2}$.

Top view of precipated Si nanoclusters
in experiment (upper image)
and simulation (lower image)

T. Müller et al. Appl. Phys. Lett. 85 (2004) 2373

Fig. 7.11

Smart Cut – Verfahren Herstellung von SOI – Wafern

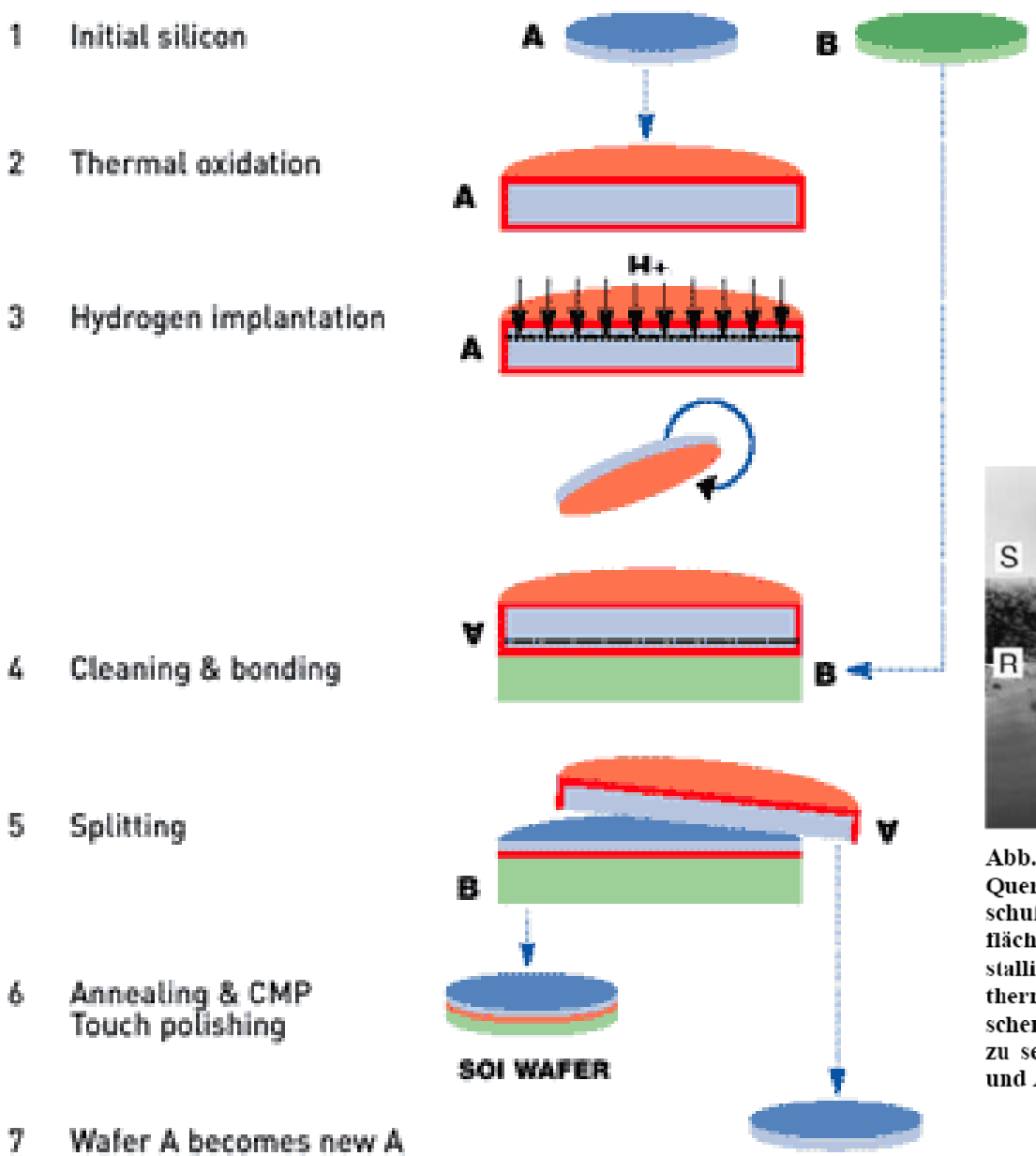

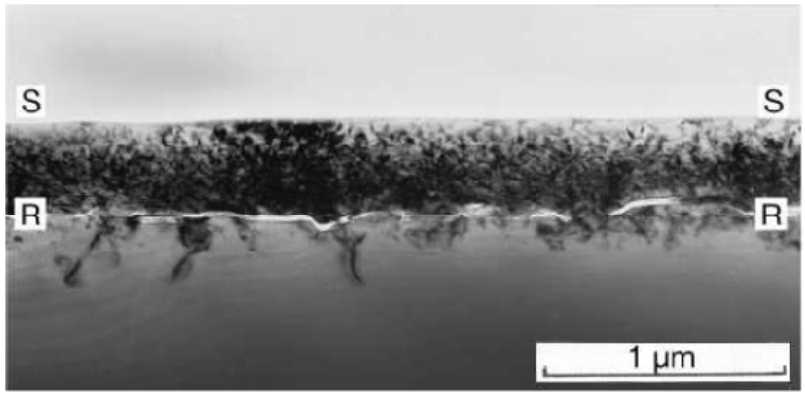

Abb. 1: Elektronenmikroskopische Durchstrahlungsaufnahme eines Querschnitts nahe der Oberfläche eines Germaniumwafers: Durch Einschuß von Wasserstoffionen und Erwärmung wurde parallel zur Oberfläche S-S ein Riß R-R erzeugt (heller Kontrast). Er trennt eine einkristalline Dünnschicht ab, die auf einen anderen Substratwafer gebondet, thermisch ausgeheilt und poliert werden kann. Im hier gezeigten Zwischenstadium sind mit dunklem Kontrast noch die Implantationsdefekte zu sehen, die anschließend thermisch ausgeheilt werden. Präparation und Aufnahme: S. Hopfe, MPI Halle

Aus: G. Kästner, Phys. Bl. 55 (1999) Nr. 1

Fig. 7.12

Nanostructure formation structure split wafer techniques

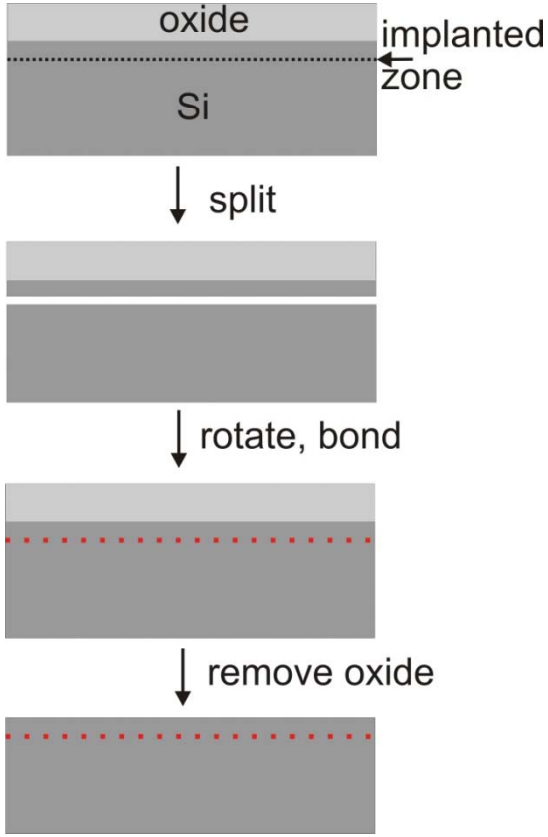

twist network
periodicity 50 nm

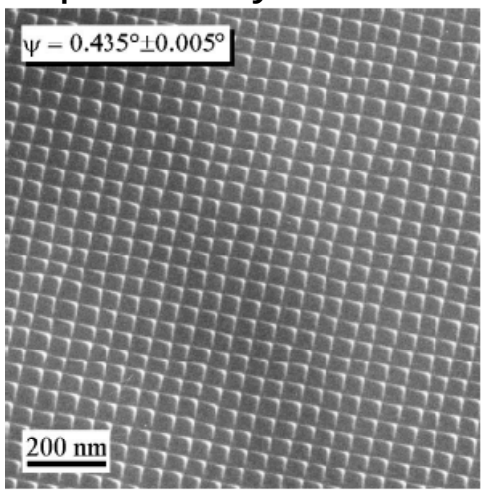

tilt network
periodicity 43 nm

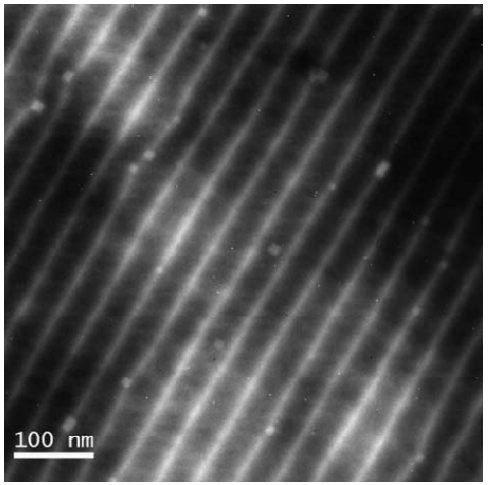

F. Fournel et al., APL 80, 793 (2002)

Fig. 7.13

The Focussed Ion Beam Microscope: Liquid Metal Source

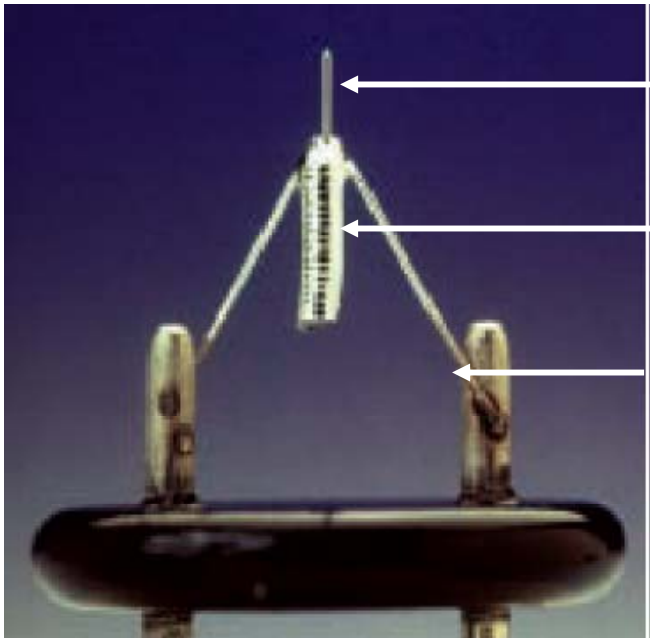

Fig. 7.14

FIB: Applications

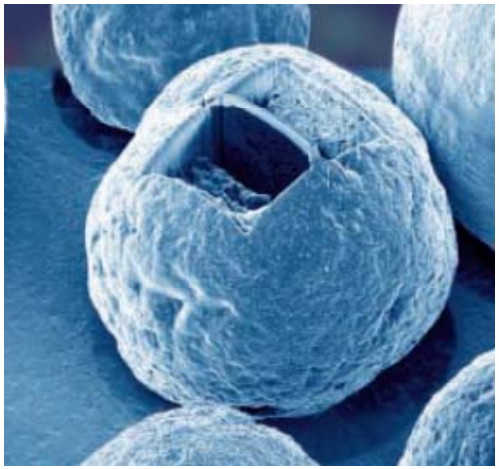

preparation of a TEM lamella from a catalyst particle

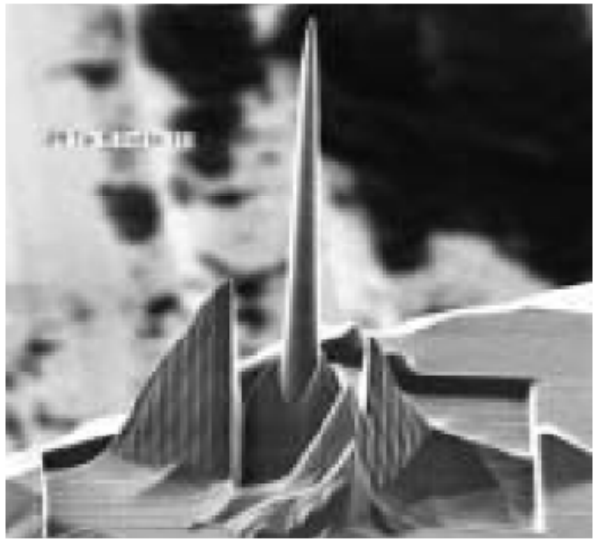

Figure 44: SE image made with FIB showing a silicon AFM tip machined to be a super-tip, with very small radius for high resolution AFM imaging.

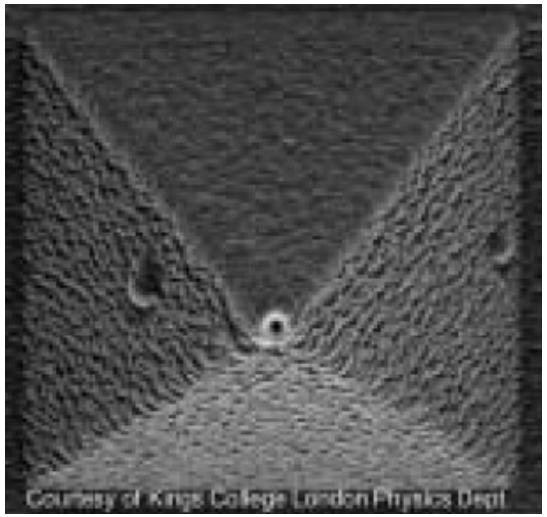

SNOM-tip

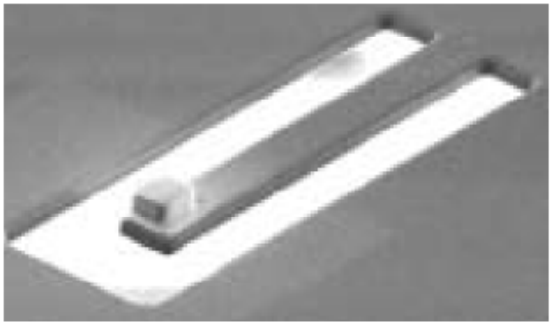

FIB machined spring in Si_2N_3 membrane

Fig. 7.15

FIB Applications

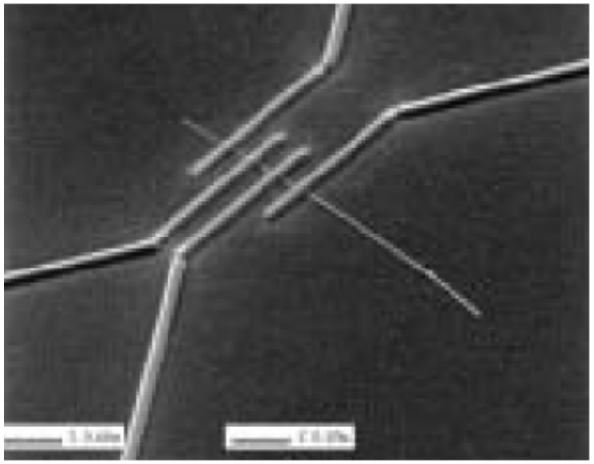

Figure 39: Ion beam deposited tungsten nano-wires for direct electrical measurements (4 point probe) of nano structures, in this case a carbon nanotube.

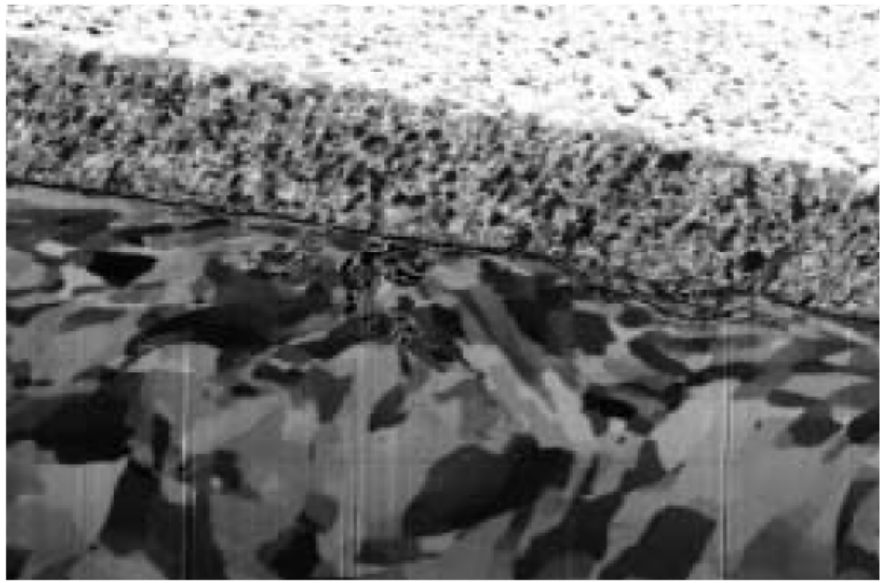

Figure 7: Ion image of a chromium coated steel wire, showing very strong contrast of the metallic grains, due to their orientations.

Fig. 7.16

Scanning Microscopy

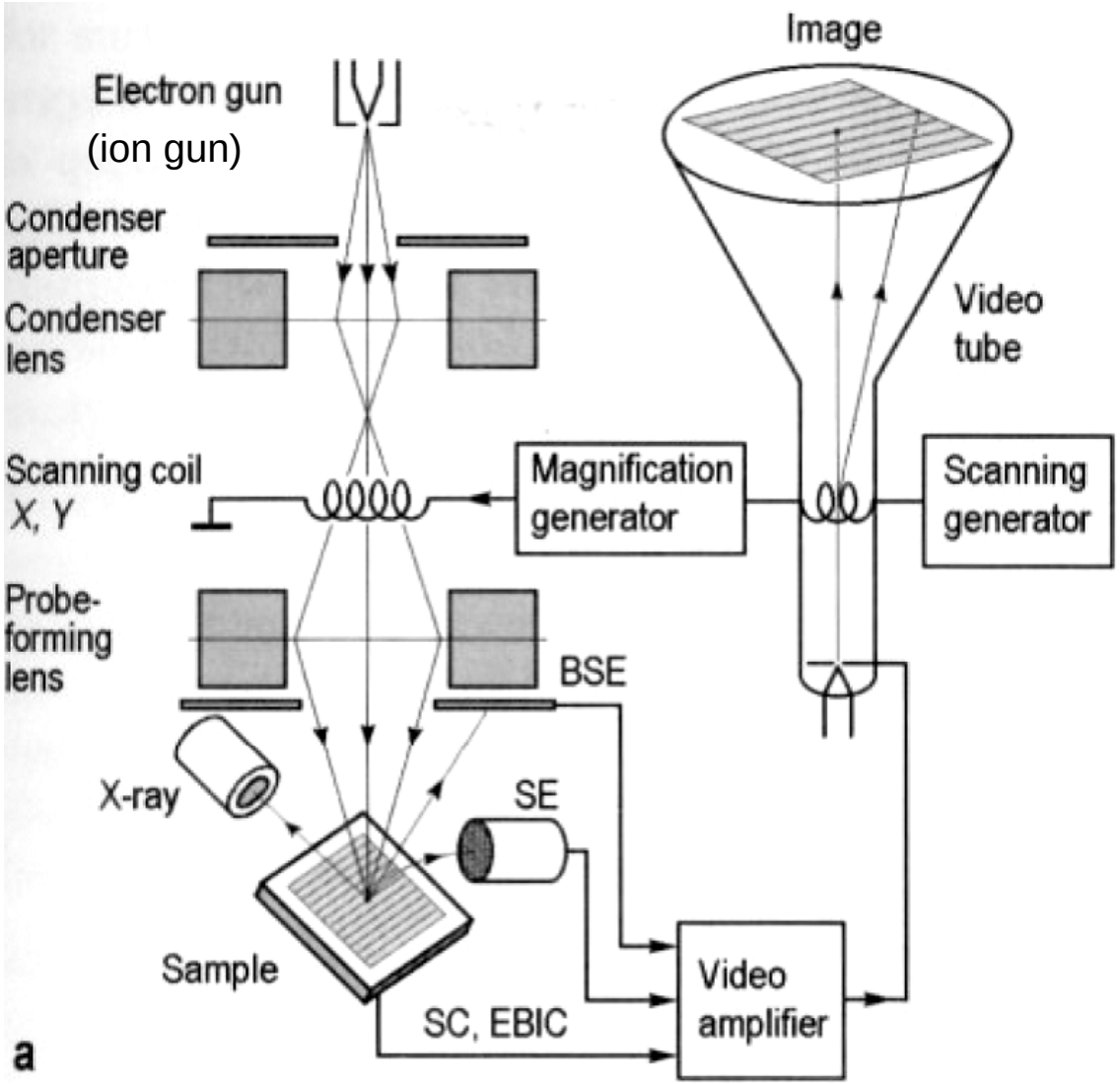

Fig. 7.17